Performance Analysis of MPBC with PI and Fuzzy Logic Controllers Applied to Solar Powered Electric Vehicle Application

RAKESH BABU BODAPATI*, R. S. SRINIVAS, P. V. RAMANA RAO
Department of Electrical and Electronics Engineering,
Acharya Nagarjuna University,
Guntur, Andhra Pradesh-522510
INDIA

*Corresponding Author

Abstract: - One of the more complicated cases is managing the energy between multiple power sources that are utilized to power electric cars (EVs). Power management is often carried out following the load requirements of electric vehicles. By considering the speed and current values of the motor a novel controller is modeled named as Measurement of parameter-based controller (MPBC) which is used to obtain the smooth transition between two passive energy sources battery and Supercapacitor (SCap). Further, the proposed MPBC is combined with fuzzy logic (FLC) and proportional-integral (PI) controllers, forming two different hybrid controllers named MPBC+FLC and MPBC+PI, utilized to attain proper power management. The main function of traditional controllers FLC/PI is to generate the pulse signals to the switches present in the bidirectional converters at both battery and SCap end. On the other hand, the MPBC is utilized to control the pulse signals based on the current and speed values of the electric motor. Futcher's final MATLAB/Simulink model is built with the proposed control technique with two hybrid controllers by considering different power-generating conditions of the PV array, to know the effectiveness of the individual model.

Key-Words: - Fuzzy Logic System, Energy Management (EMGT), Proportional Integral (PI) controller, Hybrid controller (HC), Measurement of parameter-based controller (MPBC), Electric vehicle, Battery, Photo Voltaic (PV) energy.

Received: May 8, 2023. Revised: April 6, 2024. Accepted: May 11, 2024. Published: June 3, 2024.

1 Introduction

In the future, renewable energy (RE) sources will replace conventional energy sources as the primary means of generating electricity. The use of conventional energy to produce power is getting more expensive and hurts the environment due to large emissions. The main alternative method for generating energy at a low cost and with little environmental impact is solar power generation. Here, sufficient sunlight and irradiance can be used as inputs to produce solar-powered electricity without harming the ecosystem. When solar-powered facilities generate electricity, no appreciable emissions are emitted into the atmosphere, indicating that they are environmentally benign.

These days, the conventional vehicle system is the only one that is used for a large portion of transportation. However, depending on the input energy storage system being used, this traditional vehicle system-based transport system needs to be modified. Typically, a conventional transportation system vehicle runs on petrol or diesel, both of which have limited supply and produce a significant amount of exhaust gases when in use. It will be necessary to convert to an alternative source-based vehicle to overcome the future limitations of conventional fuels. To reduce the use of fuel and diesel, battery-powered electric vehicles are being developed in place of internal combustion engine-based vehicles. Typically, to fully charge the energy source, we must plug the car in to charge the battery. This element contributes to the local electricity grid becoming overloaded once more. A solar-powered power plant is used to create a separate power-producing station within the car to reduce the load on the local grid. The local electricity grid will experience less load as a result. Renewable energy sources, such as wind, sun, and biomass, produce energy by absorbing input from a wealth of resources. For instance, throughout the day, sunshine is available, making it simple and independent to meet rising load demands. According to the results of the standard survey,

conventional technologies are capable of producing over 70% of the electricity. However, only renewable resources are used to create a maximum of 30% of the power. This does not bode well for the ecosystem. The people in the society should be educated to maximize the generation of non-conventional power. From a transportation perspective, this initiative will increase the use of EVs and reduce the load on the local grid, [1].

To fulfill the current load demand, new energy sources are of vital importance because fossil fuels are running out quickly. Trends in global warming can also be attributed to the use of fossil fuels, [2]. The most practical solution to this global energy problem is to use renewable energy sources. Electricity in the future is anticipated to be primarily supplied by RE sources, [3], [4].

Investigation of integrated energy storage management and real-time load evolution at grid-connected solar electric vehicles. Without any prior knowledge, a finite time approach with subjective dynamics of structure inputs has been taken into consideration. Through the combined optimization of EV energy ordering quantity, load planning delays, photovoltaic abundance during periods of nearby produced renewable energy, and battery deprivation, the goal is to lower a standard aggregated system price. The model of one-slot look-ahead queue stability uses the Lyapunov optimization method (LOM) to solve the problem as a result of repeated reformulation and adjustment of the combined optimization challenge, [5].

The choice of HEVs in transportation networks is becoming more attractive and important due to their increased energy consumption. Because of its eco-friendly design and support for the smart grid idea, HEVs are experiencing rapid growth. There are variations in HEV types because of the differences in ESS across various control techniques. This makes it harder to choose a suitable control approach for HEV applications. An extensive analysis of the key ESS data about HEVs and feasible optimization topologies based on various control schemes and vehicle tools, [6].

In this case, the research and analysis involve transforming the conventional vehicle system into an autonomous electric vehicle (EV). Reach out to several ESS devices, such as lead-acid and lithium-ion (Li-ion) batteries, during this procedure. Three driving cycles that match the conditions of moving in have been used in MATLAB/Simulations. These cycles include a highway with a climb up a mountain a city, and a highway. All requirements are based on highways in the Vale do Paraíba Paulista region, [7], [8].

This study observes the current ESS in EVs and HEVs, which consists of a battery and a supercapacitor, to reduce its power density scarcity. Because there are two ESSs, energy management needs to be implemented for the HESS. The best energy management strategy is created by taking into account Pontryagin's minimal principle, which instantly distributes the required impulsion power to the two ESS during vehicle propulsion and also quickly distributes the regenerative braking energy to the two ESS, [9].

The main obstacle to optimal energy management for HESS-based EVs is the development of supervisory control techniques. A multi-objective optimization model is developed to enhance the power exchange between the supercapacitor and battery. This method handles problems in an approachable and optimal manner, [10], [11].

For an EV powered by supercapacitors, a real-time combined speed control and power flow supervisory system is developed using a nonlinear control system approach. Given the relationship between energy management and HESS sizing, this work uses a controller design for HESS sizing to find the ideal HESS size to serve an EV. The controller uses the HESS selectively to reduce power consumption and traces the vehicle's set speed with uniformly exponential stability to decrease battery stress. It is necessary to use a composite controller by using the physical source of the vehicle's power requirement. To determine the use of the controller and HESS sizing system, a typical urban dynamometer driving program is used to imitate the driving cycle of a full-size EV, [12]. Finding $2n-1$ stage rearrangeable Banyan-type networks that are not isomorphic to one another is the objective of this work. This is achieved by building substitute networks and evaluating how well they can be rearranged using the satisfiability problem. The limited scalability of this strategy is a drawback because of the huge number of candidates. To eliminate this issue, it is shown that the possibilities can be reduced to a smaller class of networks called pure banyan networks. This is achieved through the use of network isomorphism analysis, [13], [14]. This study intends to evaluate the potential for fuel cell electric vehicle (FCEV) adoption in Morocco and to provide insight into fuel cell vehicles by thoroughly evaluating the Moroccan hydrogen roadmap. To determine the crucial success factor for increasing FCEV adoption in the Kingdom, a SWOT analysis was also carried out, [15], [16]. Based on an analysis of the development status of a BESS, the study presented application scenarios,

such as the reduction of power output fluctuations, acceptance of output plans at the side of renewable energy generation, power grid frequency adjustment, power flow optimization at the side of power transmission, and a distributed and mobile energy storage system at the side of power distribution, [17], [18], [19], [20].

2 Energy Storage System of Existed Model

In the current study, a single energy source that combines solar energy with built-in power generation was utilized to power the vehicle independently of the local power grid. With this setup, the EV can simultaneously charge the battery and generate power using the solar panel when there is sunlight. It indicates that the battery will supply the necessary power to the load for continuous operation when driving at night.

2.1 Battery Model

The model-based design needs only one or two iterations of changing and re-verifying the power system design. The battery is used in the wind power EV system to store the energy from the grid supply and also provide the energy to load.

2.1.1 Internal Structure of the Battery

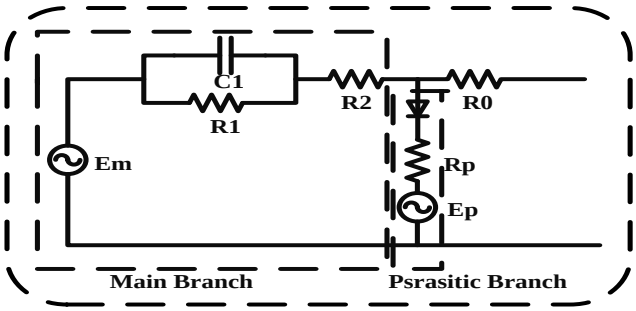

Fig. 1: Equivalent circuit of the battery

The battery's physical model is developed by taking into account several variables, including temperature, voltage, and current rating values. Figure 1 depicts the battery's electrical circuit model.

Equation (1) provides an expression for the main branch voltage.

$$E_m = E_{m0} - K_E(273+\theta)(1-SOC) \quad (1)$$

The terminal resistance R0 is expressed in equation (2).

$$R_0 = R_{00}\left[(1+A_0)(1-SOC)\right] \quad (2)$$

The main branch resistance R1 is expressed in equation (3).

$$R_1 = -R_{10}\ln(SOC) \quad (3)$$

The main branch capacitance C1 is expressed in the equation (4).

$$C_1 = \tau_1 / R_1 \quad (4)$$

The main branch resistance R2 is expressed in equation (5).

$$R_2 = R_{20}\frac{\exp\left[A_{21}(1-SOC)\right]}{1+\exp\left[A_{22}\,\mathrm{I_m}/I^*\right]} \quad (5)$$

The extracted charge of the battery is expressed in equation (6).

$$Q_e = Q_{einit} + \int -\mathrm{I_m}(\tau)dt \quad (6)$$

The normal current can be assessed by using the following equation (7).

$$I_{avg} = \frac{\mathrm{I_m}}{(\tau_1 s+1)} \quad (7)$$

2.2 Super Capacitor Model

The ultracapacitor differs from a typical capacitor in that it is constructed with a dielectric made of two plates and can store a certain quantity of energy. Because UC uses multilayer porous electrodes, which increase the layer's surface area more than a regular capacitor does, UC can store 100–1000 times more energy than a normal capacitor.

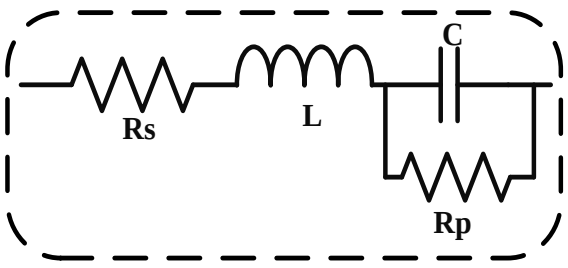

Fig. 2: General first-order model of the Supercapacitor

The general practical ultracapacitor is represented with a Figure 2, in which Rs, L, C, and Rp are connected in series and parallel. In this case, losses during the charging and discharging phases are caused by the series Rs. However, Rp also results in losses when the capacitor that is connected in parallel with it discharges. Practically from a

high-power applications point of view, the Rp value is neglected because the Rp value is much higher than the Rs value.

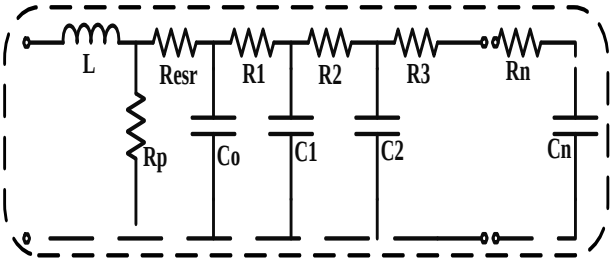

Fig. 3: Detailed model of the Supercapacitor

Based on the multilayer capacitor technology the SCap is derived, and its structure resembles the distributed network of the transmission line shown in Figure 3 so to perform the theoretical calculation of the SCap voltage-dependent capacitance model is taken as the reference.

The classical and simplified model of the SCap is represented in Figure 4. in which Rp is connected as a parallel resistance and Resr is connected as a series resistance C will be the variable capacitance Co is the constant capacitance value as treated. The total capacitance value of the SCap depends upon the voltage of the SCap, again which can be expressed in terms of variable capacitance and constant capacitance.

$$C_{cell} = C_0 + kV_C \tag{8}$$

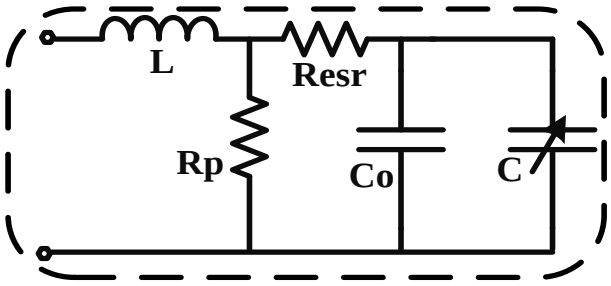

Fig. 4: A simplified model of the Ultracapacitor

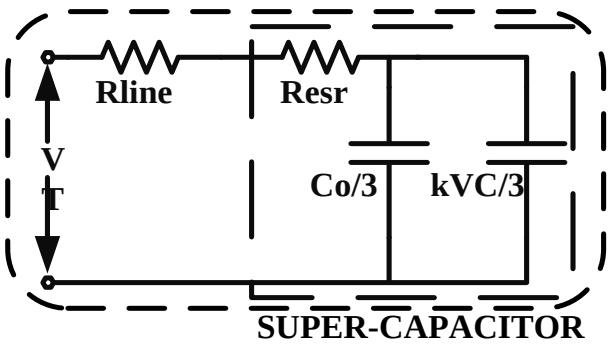

Fig. 5: Derived Equivalent Model of 6v Series Bmod0140-E048 Supercapacitor

Here Resr is the equivalent series resistance, which relates the energy losses during charge and discharging periods. Figure 5 Three different cells are considered with voltage level 2.7V each and the required total voltage level is 6V after three cells series connection. So, the capacitance for three cells in the model is given as:

$$C_{total} = \frac{1}{\frac{1}{C_{cell1}} + \frac{1}{C_{cell2}} + \frac{1}{C_{cell3}} + \text{------} + \frac{1}{C_{cell18}}} \tag{9}$$

$$C_{total} = \frac{1}{3} C_{cell} = \frac{1}{3}\left(C_0 + kV_C\right) \tag{10}$$

Equivalent resistance in series is given as:

$$\mathrm{R}_{ESR} = 3\left(\mathrm{R}_{esr}\right) \tag{11}$$

Apply Kirchhoff's voltage law (KVL) to the circuit in Figure 5 then:

$$\left(R_{line} + R_{ESR}\right) i + \frac{1}{C_{total}} \int i dt = V_T \tag{12}$$

The above equation can be expressed in differential equation form as:

$$\left(R_{line} + R_{ESR}\right) \frac{dq}{dt} + \frac{1}{C_{total}} q = V_T \tag{13}$$

Put $q = C_V$,

Then voltage value of the SCap will be,

$$\left(R_{line} + R_{ESR}\right)\left(C_0 + 2kV_C\right) \frac{dv_c(t)}{dt} + v_C(t) = V_T \tag{14}$$

or

$$\frac{dv_c}{dt} = \frac{V_T - v_c}{\left(R_{line} + R_{ESR}\right)\left(C_0 + 2kv_c\right)} \tag{15}$$

The voltage across internal resistance will be found from:

$$R_{ESR} i(t) + \frac{1}{C_{total}} \int i(t) dt = V_T \tag{16}$$

At the instant of switching, t = 0+;

$$R_{ESR} i(t) - \frac{1}{C_{total}} \int i(t) dt = V_0 \tag{17}$$

Multiply by C_{total} and take a derivative:

$$C_{total}\,\mathrm{R}_{ESR}\frac{di(t)}{dt}-i(t)=0 \tag{18}$$

Multiply by R_{ESR} and note that $v_r(t)=Ri(t)$

$$C_{total}\,\mathrm{R}_{ESR}\frac{dv_r(t)}{dt}-v_r(t)=0 \tag{19}$$

And the solution of,

$$v_r(t)=ke^{\frac{1}{R_{ESR}C_{total}}t} \tag{20}$$

Hence, the voltage across the terminal of the SCap is:

$$v_t(t)=v_r(t)+v_c(t) \tag{21}$$

and for discharging a UC is:

$$\frac{dvc}{dt}=\frac{-(vc)}{(R_{line}+\mathrm{R}_{esr})(C_0+2kvc)} \tag{22}$$

and the terminal voltage of the supercapacitor in discharging is:

$$v_t(t)=v_c(t)-v_r(t) \tag{23}$$

3 Description of Existed Model Controllers

3.1 Fuzzy Logic Controller (FLC)

The rule-based fuzzifier interface and fuzzifier are two crucial FLC phases. In addition to the MPBC controller, another controller included in the suggested control architecture is the FLC. Three blocks are essential for producing output signals in these, which are then utilized to generate the controlling signal for the converter switches which is clear from Figure 6. Here, the fuzzification block receives the change in error and error value. The fuzzy inference uses this block as its input.

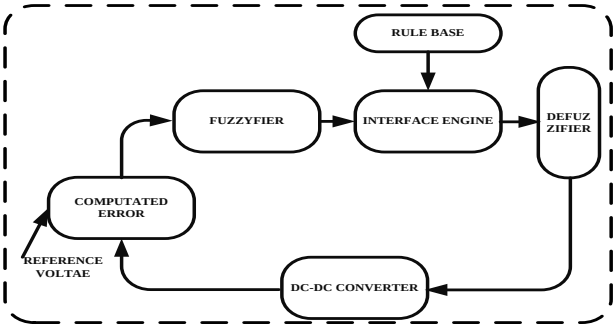

Fig. 6: Block diagram representation of FLC

3.2 PI Controller

$$P=K_pe+\frac{K_p}{T_i}\int edt \tag{24}$$

After applying the Laplace transformation:

$$P(s)=\left\{Kp\left[1+\frac{1}{T_iS}\right]\right\}E(s) \tag{25}$$

Let $e=\sin\omega t$ input

$$P=K_p\sin\omega t+\frac{K_p}{T_i}\int\sin\omega t dt \tag{26}$$

$$P=K_p\sin\omega t+\left(\frac{-K_p}{T_i}\right)\cos\omega t \tag{27}$$

$$P=\sqrt{(K_p)^2+\left(\frac{K_p}{\omega T_i}\right)^2},\sin\left[\omega t-\mathrm{Tan}^{-1}\frac{1}{(\omega T_i)}\right] \tag{28}$$

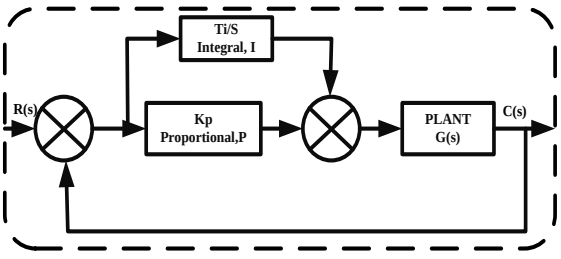

Fig. 7: Traditional block diagram representation of PI controller

PI controller with gain and plant blocks including error signal block is represent in Figure 7.

3.2.1 Implementation of the PI Controller

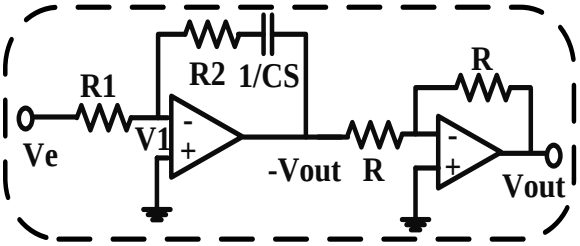

Fig. 8: Real-time implication model of PI controller

$$\frac{V_e - V_1}{R_1} = \frac{V_1 - V_{out}}{R_2 CS + 1 \diagup R_1 CS} \tag{29}$$

$$-V_{out} = \frac{V_e \left[R_2 C_S + 1 \right]}{R_1 CS} \tag{30}$$

$$-V_{out} = V_e \frac{R_2 CS}{R_1 CS} + \frac{V_e}{R_1 CS} = \frac{R_2}{R_1} V_e + \frac{V_e}{R_1 CS} \tag{31}$$

$$V_{out} = \frac{R_2}{R_1} . V_e + \frac{R_2}{R_1} . \frac{1}{R_2 C} \int V_e dt \tag{32}$$

After comparing the above expression with the standard PI controller equation:

$$K_p = \frac{R_2}{R_1} \tag{33}$$

$$T_i = R_2 C \tag{34}$$

Real time block implementation of the PI controller is shown in Figure 8, which includes different resistance, capacitor and Operational amplifiers.

4 Energy Management Strategy with Proposed Control Technique

This proposes a novel control method, SCap, based on the electric motor's speed and current values, to enable the battery to switch between its charging and discharging stages. Two distinct controllers are used to implement the suggested control technique: the typical controllers FLC and PI are employed to produce the pulse signals that are sent to the converter. Additionally, such signals are controlled by the MPBC controller by the electric motor's speed and current levels. Ultimately, the approach to fulfill the suggested technique is provided by the combination of MPBC+PI and MPBC+FLC.

The PV array, battery, SCap, two bidirectional converters, Boost converter, and the electric motor shown in Figure 9 comprise the primary circuit of the suggested model. In this case, the battery is used to supply the EV with backup power when solar power generation isn't available, while the SCap is used to fulfill the peak power requirement. In contrast, PV arrays are used, depending on the load placed on the EV, to meet the requirement for EVs as well as for battery and SCap charging. The two bidirectional converters' regulated signals are all based on the proposed control technique, which consists of two separate controller combinations known as MPBC plus PI. Based on the actual and reference voltage levels of the converter, the PI or FLC controller in this instance generates the pulse signal to the converter at the battery and SCap end. However, MPBC operates based on the EM's current and speed values. This is achieved through the use of math functions, which produce three distinct signal types depending on the EM's current and speed values. To provide the converter at the battery and SCap ends with regulated pulse signals, MPBC, PI, and FLC work together to provide the EV with the appropriate power supply based on the applied load.

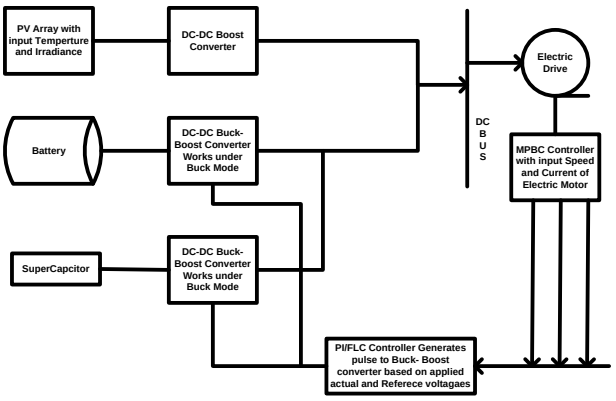

Fig. 9: Main circuit with a Proposed control technique

Here, three distinct load scenarios are taken into account, and the controlled signals to the EV are created accordingly. This will occur by the suggested controlled technique, which combines FLC, PI, and MPBC.

The EM's speed and generation-related current are described by the math functions.

1. The MPBC system creates a signal and sets Y1 to 1 and Y2 and Y3 to 0 when the speed reaches or exceeds 1500 rpm and the current remains below 6A. As a result, the supercapacitor (SCap) and the converter at the battery end function in a buck mode, making it easier to charge the battery and SCap using solar energy. Current flows from the PV array to the load, SCap (for a short while), and batteries during this procedure. In addition, the SCap releases an

equivalent amount of energy to support the motor if it encounters a high load during startup.

2. The MPBC, controller emits a signal when the speed is between 1400 and 1499 rpm and the current is between 6 and 8 amps. Y2 is then set to 1, and Y1 and Y3 are set to 0. In this case, the supercapacitor (SCap) rapidly supplies the motor with the required peak power while the converter at the battery end stays inactive. In boost mode, the converter at the SCap functions. There is no current flowing to the battery and just a brief current flowing to the load from the PV array and SCap. This suggests that during this time, the battery does not charge or discharge.
3. When the EM's speed falls below 1400 rpm and its current exceeds 8 amps, the MPBC will produce a signal of one for Y3 and zero for the other two functions. Because of this, the converter at the battery and SCap ends operated in boost mode, allowing current to flow to the load from the battery, SCap, and PV array. This shows that, up until the point of charging, the battery helps the solar array and the SCap under high-load situations.

4.1 Modes of Operation of the Main Circuit Model

Depending on the load placed on the EV, the main circuit operates in one of three modes. The various modes of operation of the main circuit about the applied load are depicted in Figure 10, Figure 11 and Figure 12.

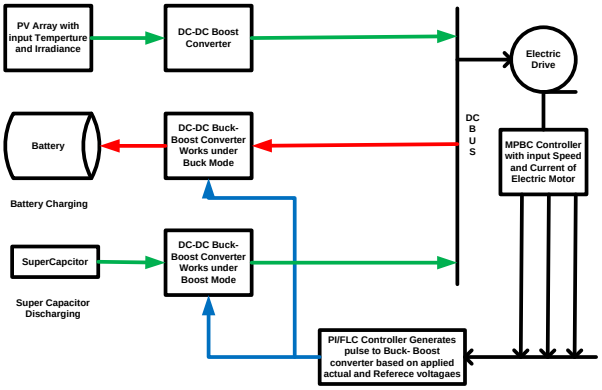

Fig. 10: The main circuit with load and battery power meet from the PV array and SCap short time.

The EV's main circuit under typical load circumstances is seen in Figure 10. In this instance, the battery can be charged by the PV array in addition to providing electrical power to the load. This suggests that controlled pulse signals are generated to the converter at the battery end to operate under the buck mode of operation, depending on the speed and current values of the electric vehicle. Here, the converter at the PV array's end operates exclusively in boost mode. This demonstrates that for mathematical function Y1, the MPBC controller will be able to generate signals as 1, and for the other two functions, as zero. In addition, the PV array is supported by the SCap when the electric motor is operating at maximum power.

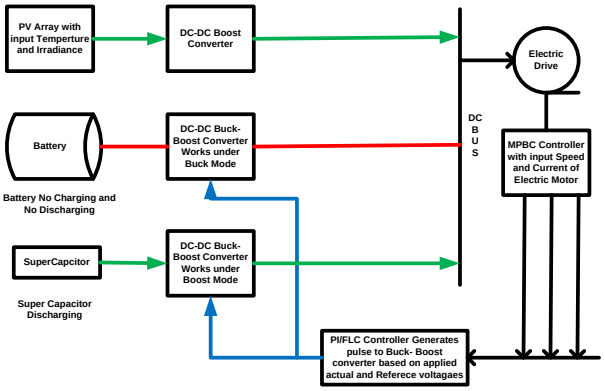

Fig. 11: The main circuit with load power meet from the PV array and SCap for a short time

Because of the rated load placed on the EM, Figure 11 depicts the main circuit power flow from the PV array to the EV only. In this instance, the MPBC controller uses the suggested control approach to regulate the pulse signals produced by the PI or FLC. As a result, for the remaining math functions, the MPBC will develop the Y2 function as 1 and 0. The battery is neither charged nor discharged when operating in this mode since the converter at the battery is in the no-working zone. In addition, the PV array is supported by the SCap when the electric motor is operating at maximum power.

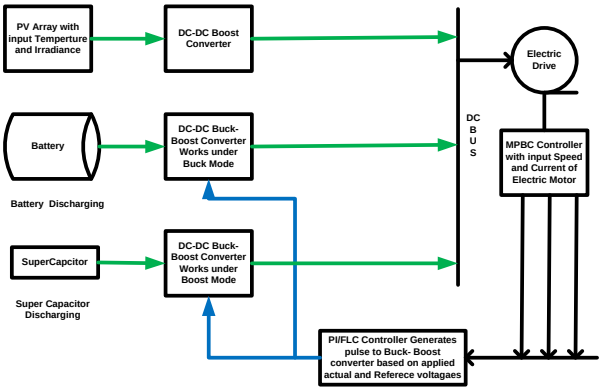

Fig. 12: The main circuit with load power meet from the PV array and battery

The main circuit current flow from the PV array plus batteries to the load is shown in Figure 12. This demonstrates the high load that the EV is subjected to because the battery supports the PV array by supplying more power to the load as needed. Furthermore, the PI or FLC-generated pulses are controlled and supplied to the converter at the battery end to perform the boost operation only because the MPBC controller can generate the signal as 1 for math function Y3 and zero for the remaining two functions, Y1, Y2. In addition, the SCap operates in boost mode on the electric motor and converter to support the PV array at peak power conditions.

5 Simulation Results and Analysis

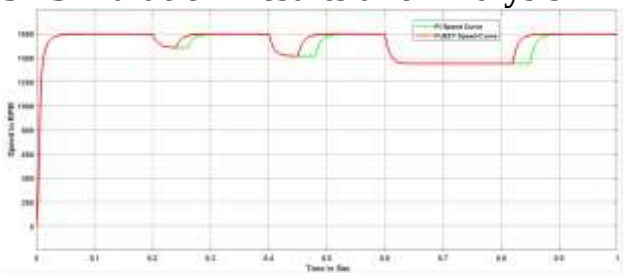

Fig. 13: Electric motor speed curve representation under various load scenarios using PI and FLC

Figure 13 shows the speed curve response of EM under various loads. Here, three distinct loads are delivered to the EV at three separate times to confirm the efficacy of the suggested control method. When a normal load is applied to the EM for 0.2 seconds, the motor's speed decreases to about 1500 rpm. When a rated load is applied for 0.4 seconds, the motor's speed decreases to 1400 rpm. Finally, when a 0.6-second extra rated load is applied, the motor's speed decreases to even less than 1400 rpm. While MPBC+FLC took 0.075 seconds, 0.08 seconds, and 0.28 seconds to attain stability in accordance with the applied loads in order, MPBC+PI took 0.09 seconds, 0.1 seconds, and 0.30 seconds. The results from the two controller outputs showed that MPBC plus FLC performed better.

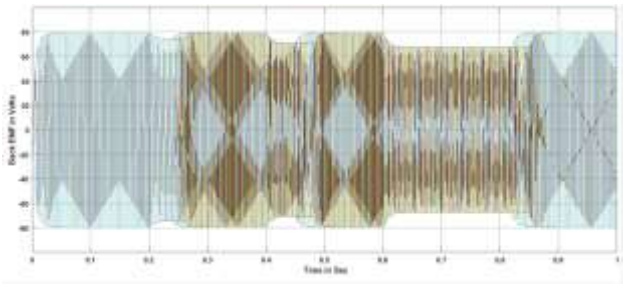

Fig. 14: Electric motor's back EMF under various load scenarios using PI and FLC

The electric motor's back EMF curve under various load scenarios is displayed in Figure 14. This will follow the speed curve: at 0.2 seconds, the curve appears to be decreasing and eventually achieves the steady state; at 0.4 seconds, the EM's rated load condition causes the back emf to fall for a while before reaching the steady state once more. Eventually, at 0.6 seconds, the motor's overrated load causes the rear emf value to drop significantly once more. This process will continue for some time before returning to its steady-state value, all because of the suggested control strategy.

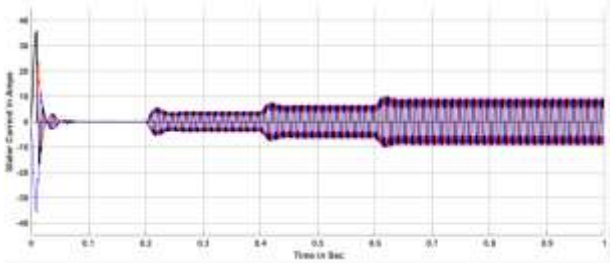

Fig. 15: Electric motor current changes related to load.

Figure 15 shows the electric motor current under varying load levels. The motor draws a significant amount of current at first, but after it reaches a steady state, that value drops to nominal, meaning the motor is operating without a load. Different types of loads are applied to the EM at 0.2, 0.4, and 0.6 seconds, which causes the motor to draw more current in proportion to the imposed load—6A, 8A, and more than 8A.

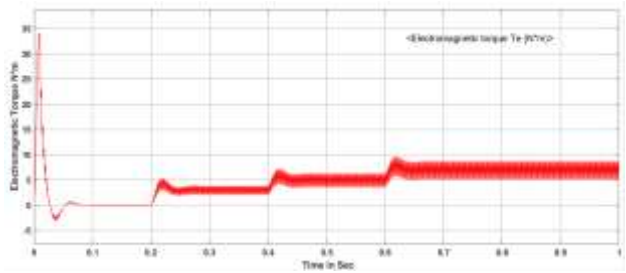

Fig. 16: Load changes representation on the Electric Motor

The load curve representation on the EM is displayed in Figure 16. The motor has a heavy load before reaching a steady state, therefore EM will require more current than at regular intervals. Figure 12 makes it clear that the motor reaches a steady state at 0.1 seconds, at which point no load will manifest itself in the motor. To assess the

effectiveness of the suggested control method, varying loads are applied for 0.2, 0.4, and 0.6 seconds. As a result, the motor's speed reduces and the current drawn by the EM increases in combination.

Table 1. Performance comparison between MPBC plus PI and MPBC plus FLC based on the speed value

S.No	Controller Name	Time Taken to reach Steady state in sec		
		Mode1	Mode2	Mode3
1	MPBC+PI	0.09	0.1	0.30
2	MPBC+FLC	0.075	0.08	0.28

Table 1 represents the comparison analysis between MPBC plus PI and FLC based on the speed curve settling value. And which clear MPB plus FLC has given better performance compared to MPBC plus PI.

6 Conclusion

This work examines a control mechanism that modifies the battery and SCap concerning the motor's speed. Three different math functions that are independently realized based on the motor's speed and current values are combined to create the MPBC. The proposed MPBC controller is combined with a traditional PI controller and FLC to create a hybrid controller to fulfil the primary goal of the project. The MFBC regulated the pulse signals that corresponded to the motor speed, while the PI controller FLC generated the switching signals needed by the converter. Ultimately, a smooth transition between battery and SCap is achieved by the demands of electric vehicles by using the suggested control approach. To carry out the same function as MFB with PI controller, another hybrid controller called MPBC with FLC is devised. When applying the afterload and starting, a comparison study is carried out. The final section contains a tabulation and presentation of the findings for all two techniques. Ultimately, the performance of the MPBC plus FLC was superior to that of the other hybrid controller, MPBC+PI.

References:

[1] A. S. Abdelaal, S. Mukhopadhyay and H. Rehman (2022). Battery Energy Management Techniques for an Electric Vehicle Traction System in *IEEE Access*, vol. 10, pp. 84015-84037, doi: 10.1109/ACCESS.2022.3195940.

[2] H. -B. Yuan, W. -J. Zou, S. Jung and Y. -B. Kim (2022). A Real-Time Rule-Based Energy Management Strategy with Multi-Objective Optimization for a Fuel Cell Hybrid Electric Vehicle in *IEEE Access*, vol. 10, pp. 102618-102628, doi: 10.1109/ACCESS.2022.3208365.

[3] Rehman, W. U., Bhatti, A. R., Awan, A. B., Sajjad, I. A., Khan, A. A., Bo, R., & Oboreh-Snapps, O. (2020). The penetration of renewable and sustainable energy in Asia: A state-of-the-art review on net-metering. *IEEE Access*, 8, 170364-170388, doi: 10.1109/ACCESS.2020.3022738.

[4] Z. Ali, G. Putrus, M. Marzband, H. R. Gholinejad, K. Saleem and B. Subudhi (2022). Multi objective Optimized Smart Charge Controller for Electric Vehicle Applications," in *IEEE Transactions on Industry Applications*, vol. 58, no. 5, pp. 5602-5615, doi: 10.1109/TIA.2022.3164999.

[5] Qazi, A., Hussain, F., Rahim, N. A., Hardaker, G., Alghazzawi, D., Shaban, K., & Haruna, K. (2019). Towards sustainable energy: a systematic review of renewable energy sources, technologies, and public opinions. *IEEE access*, 7, 63837-63851, doi: 10.1109/ACCESS.2019.2906402.

[6] Candidus U. Eya, Ayodeji Olalekan Salau, Sepiribo Lucky Braide, S. B. Goyal, Victor Adewale Owoeye, Oluwafunso Oluwole Osaloni (2022). Assessment of Total Harmonic Distortion in Buck-Boost DC-AC Converters using Triangular Wave and Saw-Tooth based Unipolar Modulation Schemes. *WSEAS Transactions on Power Systems.* 17:324-338, https://doi.org/10.37394/232016.2022.17.33.

[7] Katuri, R., & Rao, G. (2023). Design and Comparative Analysis of Controllers Implemented to Hybrid Energy Storage System Based Solar-powered Electric Vehicle. *IETE Journal of Research*, 69(7), 4566–4588, doi: 10.1080/03772063.2021.1941328.

[8] dos Santos, G. S., Grandinetti, F. J., Alves, R. A. R., & de Queiróz Lamas, W. (2020). Design and simulation of an energy storage system with batteries lead acid and lithium-ion for an electric vehicle: Battery vs. conduction cycle efficiency analysis. *IEEE*

Latin America Transactions, 18(08), 1345-1352, doi: 10.1109/TLA.2020.9111669.

[9] S. Li, P. Zhao, C. Gu, J. Li, D. Huo and S. Cheng (2023).Aging Mitigation for Battery Energy Storage System in Electric Vehicles.*in IEEE Transactions on Smart Grid*, vol. 14, no. 3, pp. 2152-2163, doi: 10.1109/TSG.2022.3210041.

[10] Zheng, C., Li, W., & Liang, Q. (2018). An energy management strategy of hybrid energy storage systems for electric vehicle applications. *IEEE Transactions on Sustainable Energy*, 9(4), 1880-1888, doi: 10.1109/TSTE.2018.2818259.

[11] Katuri, R., & Gorantla, S. (2020). Realization of prototype hardware model with a novel control technique used in electric vehicle application. *Electrical Engineering*, 102(4), 2539-2551, DOI: 10.1007/s00202-020-01052-0.

[12] Shen, J., & Khaligh, A. (2015). A supervisory energy management control strategy in a battery/ultracapacitor hybrid energy storage system. *IEEE Transactions on Transportation Electrification*, 1(3), 223-231, doi: 10.1109/TTE.2015.2464690.

[13] Cao, J., & Emadi, A. (2011). A new battery/ultracapacitor hybrid energy storage system for electric, hybrid, and plug-in hybrid electric vehicles. *IEEE Transactions on Power Electronics*, 27(1), 122-132, doi: 10.1109/TPEL.2011.2151206.

[14] Satoru Ohta (2023). Necessary Conditions and Empirical Observations for Rearrangeable Banyan-Type Networks. *WSEAS Transactions on Circuits and Systems*, 22, 180-194, https://doi.org/10.37394/23201.2023.22.21.

[15] Khaldi Hamza, Mounir Hamid, Boulakhbar Mouaad (2022). A Review of Future Fuel Cell Electric Vehicles and Challenges Related to Morocco. *WSEAS Transactions on Power Systems.* vol. 17, pp.339-353, https://doi.org/10.37394/232016.2022.17.34.

[16] X. Li and S. Wang (2021). Energy management and operational control methods for grid battery energy storage systems.*in CSEE Journal of Power and Energy Systems*, vol. 7, no. 5, pp. 1026-1040, doi: 10.17775/CSEEJPES.2019.00160.

[17] Yao Zhong; Xiangjun Li; Yulong Wang; Longtao Su; Wan Jiang; Jianxiang Zhou (2021). Energy Management Method of Electricity Heat Hydrogen Multi-Coupling System for Retired Power Battery Echelon Utilization in Microgrids. *in IEEE Transactions on Applied Superconductivity*, vol. 31, no. 8, pp. 1-5, doi: 10.1109/TASC.2021.3110471.

[18] Alexander Zemliak (2023). Analysis of Some Special Functions for a Problem of Optimization of Analog Circuits. *WSEAS Transactions on Circuits and Systems*.22, 98-110, https://doi.org/10.37394/23201.2023.22.12.

[19] M. A. Izumida Martins, L. B. Rhode and A. B. D. Almeida (2022). A Novel Battery Wear Model for Energy Management in Microgrids. *in IEEE Access*, vol. 10, pp. 30405-30413, doi: 10.1109/ACCESS.2022.3160239.

[20] Zhang, L., Ye, X., Xia, X., & Barzegar, F. (2020). A real-time energy management and speed controller for an electric vehicle powered by a hybrid energy storage system. *IEEE Transactions on Industrial Informatics*, 16(10), 6272-6280, doi: 10.1109/TII.2020.2964389.

Contribution of Individual Authors to the Creation of a Scientific Article (Ghostwriting Policy)

The authors equally contributed in the present research, at all stages from the formulation of the problem to the final findings and solution.

Sources of Funding for Research Presented in a Scientific Article or Scientific Article Itself

No funding was received for conducting this study.

Conflict of Interest

The authors have no conflicts of interest to declare.